Contents lists available at ScienceDirect

Inorganic Chemistry Communications

journal homepage: www.elsevier.com/locate/inoche

Short communication

Co-sensitization effect of N719 dye with Cu doped CdS colloidal nanoparticles for dye sensitized solar cells

Anurag Roy [a,*], M.J.S. Mohamed [b], M.A. Gondal [b,c,*], Tapas K. Mallick [a], Asif Ali Tahir [a], Senthilarasu Sundaram [d]

[a] *Environment and Sustainability Institute, Faculty of Environment, Science and Economy, University of Exeter, Penryn Campus, Cornwall TR10 9FE, United Kingdom*
[b] *Laser Research Group, Physics Department, King Fahd University of Petroleum and Minerals (KFUPM), Dhahran 31261, Saudi Arabia*
[c] *K.A. CARE Energy Research and Innovation Center, King Fahd University of Petroleum and Minerals (KFUPM), Dhahran 31261, Saudi Arabia*
[d] *Electrical and Electronics Engineering, School of Engineering and the Built Environment, Edinburgh Napier University, Merchiston Campus, Edinburgh EH10 5DT, United Kingdom*

A B S T R A C T

Dye-sensitized solar cell's (DSSC) performances are enhanced by engineering the materials at the interface of various device components owing to easy and inexpensive fabrication steps. Ru (II) polypyridyl-based synthetic dyes are the most widely used photosensitizers for DSSCs due to their superior molar extinction coefficient and facile interaction with metal oxide electrodes. However, these dyes are mostly expensive, and as a result, natural dyes and metal-free organic dyes have become an alternative way for sensitization to reduce the significant drawbacks of synthetic dyes. In this study, minimizing the usage of the N719 dye can be performed through an alternative method for better light-harvesting through supreme optical interfacial interaction with colloidal Cu-doped CdS as a co-sensitizer in a facile approach. This co-sensitization signifies the colloidal CdS (donor), which can corroborate the energy transfer mechanism with the N719 dye (acceptor). The introduction of Cu causes extreme tuning of broad absorption to near-infrared for CdS, enhancing the solar light harvesting entrapment followed by extensive optical interaction with N719 dye. This accelerates the activity of the sensitizers for light absorption enhancement and expects a better performance of DSSC compared to traditional sensitization. A massive improvement in photocurrent density (~42 %) was observed without sacrificing other photovoltaic parameters, as observed for TiO₂-based photoanodes. The sensitizer's interfacial optical energy transfer process, unless excited electron recombination, may indirectly be used as an excitation source of the acceptor and minimizes the recombination energy loss.

1. Introduction

Considering several important dye-sensitized solar cells (DSSCs) device high-performance output parameters, it is necessary to understand the fundamental strategies to enhance its noticeable performance. The fundamental advantage of DSSCs lies in higher solar-to-electricity conversion efficiencies with lower production costs, flexibility and eco-friendliness [1]. The key idea of the photoelectrochemical technology closely resembles the natural photosynthesis process. Like chlorophyll in plants, a monolayer of dye molecules (sensitizer) absorbs the incident light, generating positive and negative charge carriers in the cell. Therefore, DSSC provides a technically and economically credible alternative concept to present-day p-n junction photovoltaic (PV) devices. Nanostructured semiconductor films are the framework of the photoanodes in DSSC. In contrast, appropriate dye molecules are the most critical component that ideally absorbs the most light on the semiconductor surface. Ruthenium(II) sensitizers, specially Di-tetrabutylammonium *cis*-bis(isothiocyanato)bis(2,2′-bipyridyl-4,4′-dicarboxylato)ruthenium(II) also known as N719, were exclusively used in DSSC [2]. However, their use has become limited because of their high cost and less durability due to the presence of two or three isothiocyanate (NCS) groups and the absorption maximum being restricted to 550 nm [3]. Later, metal-free organic and natural dyes were suitable low-cost sensitizers for DSSC applications. However, they are

experiencing lesser absorption and a more extended period of dye soaking that reflects lesser photocurrent generation [4]. In that scenario, natural and metal-free organic dyes have become an alternative sensitisation method to reduce synthetic dyes' significant drawbacks. However, the adsorption ability and performance evaluation were weaker than the synthetic metal–organic dyes [5]. They also exhibit weaker light stability than metal-based sensitizers; hence, the co-sensitization strategy is applied to broaden the light absorption spectra.

At this point, minimising the usage of the N719 dye can be performed through an alternative way for better light harvesting. CdS and N719 dye have been established as pronounced sensitizers in conventional quantum dot solar cells (QDSSCs) and DSSC. To find out the appropriate combination of QDSSC with DSSC, we have tried to develop a co-sensitization technique with a popular sensitizer, CdS, in QDSSC and a traditional sensitizer, N719 dye in DSSC [6,7]. This report explores a facile synthesis of colloidal Cu doped CdS nanoparticles in a bio-templating mediated process using Bovine serum albumin (BSA) protein. BSA provides functionalization of CdS to make it colloidal and can exhibit facile electrostatic interaction with the N719 dye molecules [8]. In addition, this may further exhibit the desired emission of CdS which can corroborate the energy transfer mechanism with the dye (acceptor). The particle size reduction can primarily be controlled using organic capping agents, polymers, surfactants, etc. Here, BSA is employed as a natural bio-templating agent to control the particle size and further functionalize the CdS for the desired emission. The introduction of Cu causes extreme tuning of extended absorption for CdS, enhancing the solar light harvesting entrapment. One of the initial conditions applied for a plausible energy transfer process between a donor–acceptor pair is that the donor's emission spectra must overlap to a certain extent with the acceptor's absorption [9,10]. Thus, designing the specific acceptor or donor is essential for superior spectral overlap. This donor–acceptor interaction is further expected to develop a spectroscopic interfacial process called resonance energy transfer (RET), which accelerates the activity of the sensitizers towards the enhanced performance of DSSC [10].

Several reports show a strong influence of QDs co-sensitization with the N719 dye molecules to improve photoelectric properties [11–14]. However, most of them are unclear about the optical interaction processing during the co-sensitization that enhances the electrical efficiency. Dissanayake et al. (2021) employed PbS/CdS QDs and N719 dye for co-sensitization, raising the device's electrical performance through the mixed cation effect [15]. Lin et al. (2017) reported the energy transfer effect for a DSSC in the case of N719 molecules allowing for a co-adsorption with the 1,8-naphthalimide derivative [16]. The device's efficiency has been improved by 10.8 % and 21 % under one sun (AM1.5G) upon this co-sensitization. There is a 37 % increase in the photoconversion efficiency (PCE) of the CdSe-QD co-sensitized DSSC compared with the DSSC sensitized only by the N719 dye [17]. Utilizing bisensitizer layer cell consisting of a nanocrystalline TiO_2/CdS QD/ amorphous TiO_2/N719 dye, Shalom et al. (2010) obtains a 250 % increase in cell efficiency compared to a QD monolayer cell [18].

In order to continue such an excellent interfacial strategy to improve DSSC performance, we have investigated a facile and effective approach of green emissive colloidal Cu doped CdS serves as an energy transfer candidate to receive the resonance energy N719 dye, and hence strongly provides better photon absorption on the photoanode. Through the process, unless excited electron recombination, it is indirectly used as an excitation source of the acceptor and minimises the recombination energy loss. Moreover, this donor–acceptor couple has exhibited synergistic interaction and a higher overlap with the solar spectrum without damaging the electron collection efficiency, which significantly enhances the light-harvesting efficiency of N719 dye, expected to enhance the performance of a DSSC device.

2. Experimental section

2.1. Materials

All the chemicals were used with analytical grade. Cd $(NO_3)_2$, $3H_2O$, Na_2S, $7H_2O$ flakes, Zn $(NO_3)_2$, $6H_2O$ and NaOH pellets were purchased from Merck Limited, Germany. Bovine Serum Albumin was used from Sigma Aldrich, and the suspension was stored at 4 °C. The water was used here in double-distilled water. Ethanol was used from Merck, Germany, as a washing liquid and a dispersion medium for characterization and cell fabrication.

2.2. Synthesis of Cu-doped CdS nanoparticles

The synthesis of colloidal CdS nanoparticles was adopted from the previous work [8]. Similarly, the colloidal Cu doped CdS nanoparticles have been synthesized using bovine serum albumin (BSA) mediated process under sonication. Ethanolic solution of 1, 3 and 5 mol wt% of Cu $(NO_3)_2$ was added with 0.1 M Cd$(NO_3)_2$, $4H_2O$ and 1.25×10^{-6} M (BSA) under constant sonication in an ultrasonic probe (Rivotek-30 kHz-250 W) for 45 mins and immediately after that an aqueous solution of 0.1 M Na_2S was added dropwise until the pH of the resultant solution reached 4.18.

2.3. Co-sensitized solar cell fabrication

The N719 dye-sensitized and Cu-CdS co-sensitized devices were prepared using P25 TiO_2 nanoparticles (Merck, Germany) and followed the protocol reported in our earlier works [8,19]. Usually, 0.5 mM of N719 dye is used for DSSC fabrication; however, to reduce the concentration of the N719 dye molecule; consequently, the amount was reduced to 0.1 mM during the co-sensitization process. The overall co-sensitization process was schematically described as Scheme 1.

2.4. Material characterizations

The dried powder was characterized for structural properties by powder and film X-ray diffraction (XRD) analysis on an X'pert pro MPD XRD of PANanalytical with Cu K$_\alpha$ radiation ($\lambda = 1.5406$ Å), respectively. Fourier transform-infrared (FTIR) spectra have been measured between 4000 and 400 cm^{-1} with 200 scans on a NICOLET 5700 Fourier Transform infrared (FTIR) spectrometer with a resolution of 4 cm^{-1} with the dried powder. Raman spectra were obtained using STR500, Cornes Technologies, formerly known as Seki Technotron, to evaluate the powder samples 514.5 Ar$^+$ green lasers were used with 50 mW power. The ultraviolet (UV)-visible (UV–vis) absorption spectra and diffuse reflectance (DR) spectra were measured on the powder's UV–vis-near infrared (NIR) spectrometer (Shimadzu UV-3600). The optical properties of the powder were further evaluated by recording the room-temperature photoluminescence spectrum (PL) on a steady-state spectrofluorometer (QM-40, Photon Technology International, PTI) using a Xenon lamp (150 W) as an excitation source and band-pass of 5 nm. The morphological study was monitored using transmission electron microscopy (TEM), carried out on a Tecnai G2 30ST (FEI) high-resolution transmission electron microscope operating at 300 kV. X-ray photoelectron spectroscopy (XPS) measurements were carried out on a PHI 5000 Versa probe II scanning XPS microprobe (ULVAC-PHI, U.S.) [20]. Transient photocurrent response test for all the devices was conducted utilising the Metrohm Autolab (PGSTAT302N) workstation under different light illumination sources. The utilised AAA solar simulator is manufactured by WACOM [Model no. WXS-210S-20]. WACOM solar simulator consists of Xenon short-arc lamp and two filters (UV and AM 1.5) to emulate a solar irradiance approximately to AM 1.5, as in Fig. S1, SI. External quantum efficiency (EQE) was performed on a Bentham PVE300 Photovoltaic EQE instrument.
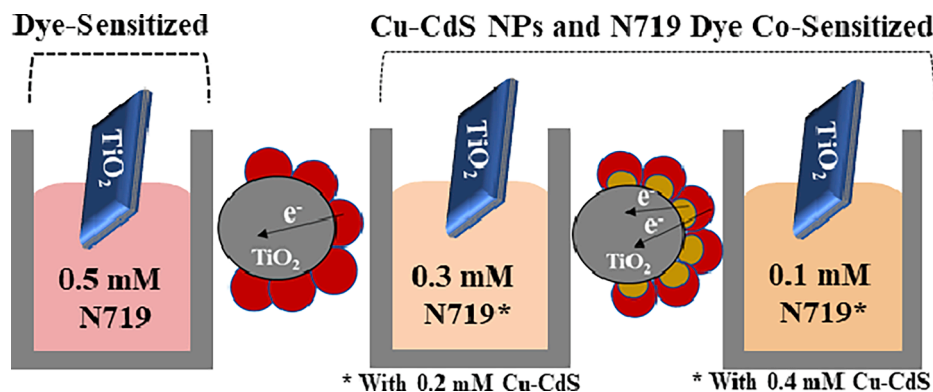
Scheme 1. Schematic representation of Cu-CdS co-sensitization process through a reduction of N719 dye concentration for TiO₂-based photoanode.

3. Results and discussion

3.1. Structural and optical analysis

The XRD patterns of the synthesized undoped CdS and 0.5,1,3 and 5 % of Cu doped CdS powders have been represented in Fig. 1a, and all of them are matched well with the reported reference pattern of cubic CdS (JCPDS card 42–1411) [21]. Doping leads to a reduction of the unit cell length (l) of the CdS crystal lattice, and as a consequence, the noticeable contraction in the unit cell volume (V) for the Cu doped samples was observed as given in Table 1. Also, Fig. 1a indicates that the intensity of the secondary CuS phase became predominant in the case of 5 % Cu doping, leading to forming of a CuS-CdS composite instead of Cu doped CdS. During doping with 3 and 5 % of Cu in a CdS crystal, a slightly lower shifting of $2\theta^o$ was observed, as shown in Fig. 1b. This lower shifting may ascertain a fruitful substitution of Cd^{2+} of the lattice sites

Table 1
Calculated lattice parameters of synthesized colloidal cubic CdS and Cu doped CdS.

Sample	Lattice Parameter (Å)	Intensity Ratio (111/200)	V(Å)³
CdS	5.817	2.05	196.83
0.5 % Cu doped CdS	5.815	2.09	196.62
1 % Cu doped CdS	5.813	3.23	196.42
3 % Cu doped CdS	5.812	3.44	196.32
5 % Cu doped CdS	5.809	3.70	196.02
JCPDS 36–1451	5.818	4.54	196.93

having a larger ionic radius of 0.95 Å by Cu^{2+} with a smaller ionic radius of 0.73 Å (Table 1) [20]. The broadness and an intense peak of the XRD reflections indicate the finer size of the formed powders having a mean
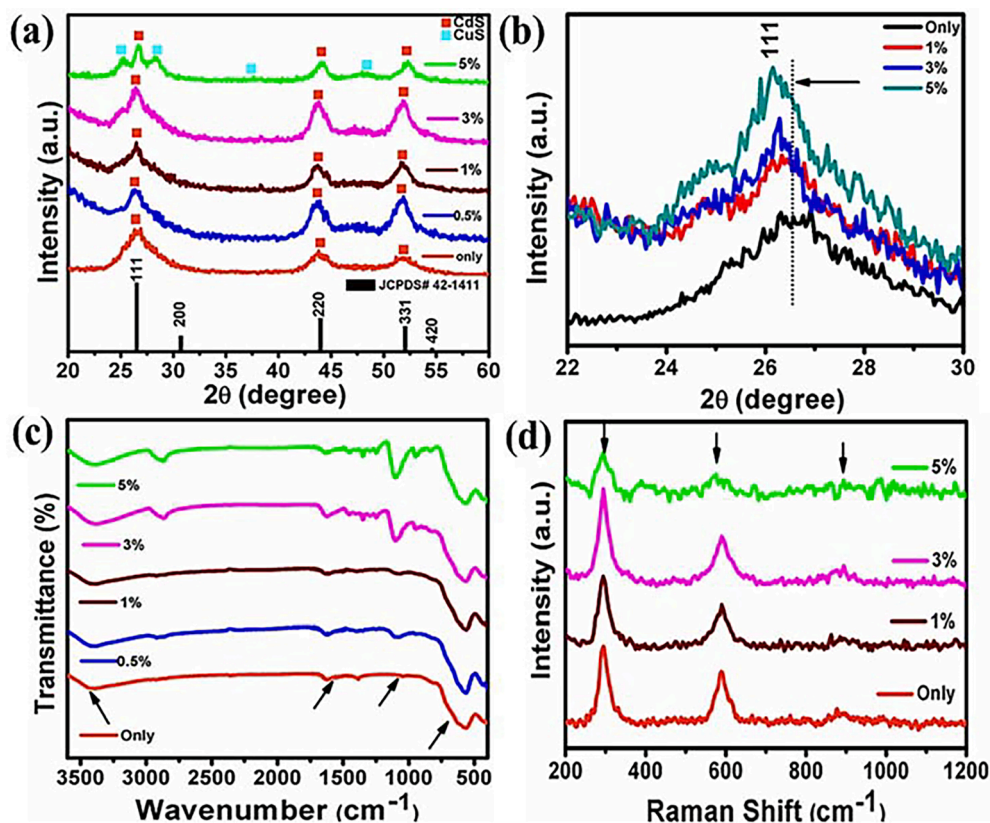
Fig. 1. (a) X-ray diffraction patterns for 0.5, 1, 3 and 5% Cu doped CdS and CdS along with standard JCPDS card no. 42-1411, (b) close X-ray diffraction pattern of cubic (1 1 1) plane for the same, (c) and (d) corresponding FT-IR and Raman spectra of the same powders, respectively.

crystallized size between 5.1 and 4.4 nm as calculated from the Scherer equation [22]. Enhancing peak intensity and reduction of crystalline size manifest successful Cu^{2+} doping in a CdS nanocrystal by remaining negligible switching of full-width half maxima of the peak. The FTIR analysis also revealed the peak assigned at 621, 1160 and 1635 cm^{-1} attributes to the Cd—S, S—H and O—H stretching vibration modes, as shown in Fig. 1c. The surface functionalization of CdS exhibited a band at ~3480 cm^{-1} due to labile —OH stretching of surface adsorbed water which is extensively making colloidal CdS for facile hydrophilic dispersion [23].

Further, the Raman study was also performed, as shown in Fig. 1d, exhibited the fundamental band (1LO) and corresponding overtone (2LO) of longitudinal optical (LO) and combination of (1LO + 2LO) phonon modes of CdS located at ~292, 590 and ~874 cm^{-1}, respectively [24]. A gradual enhancement followed the intensity according to to increment Cu^{2+} concentration from 1 to 3 %. Whereas in the case of 5 % Cu doping, the signature bands of CdS affected to a lesser extent due to the initiation of CuS-CdS composite cubic phase as observed from the XRD analysis.

3.2. Transmission electron microscopy analysis of 3 % colloidal Cu doped CdS nanoparticle

The bright-field images of 3 mol% Cu doped colloidal CdS nanoparticles (NP) were shown in Fig. 2a and b. The average particle size was calculated at ~10.2 nm corresponding to Fig. 2b. Good crystallinity and monodispersity are evident from the high-resolution TEM (HRTEM) images showing clear crystalline (1 1 1) plane lattice fringes with a lattice interplanar distance value of 0.336 nm of cubic CdS in Fig. 2c. The discrete bright spots in selected area electron diffraction (SAED) patterns reveal well-crystallized cubic form in the CdS nanoparticles with the major crystalline planes (3 1 1), (2 2 0), and (1 1 1) of cubic CdS as shown in Fig. 2d.

3.3. Absorption and photoluminescence study

The optical absorption spectra of the Cu doped CdS have been exhibited in Fig. 3a. The onset absorption edge at 482 nm for the undoped CdS has a significant bathochromic shift towards 455 nm observed only for the other % of Cu doped CdS NCs with the maximum shifting for 3 % Cu doping. Besides, insignificant shifting was observed in the case of 5 % Cu doping. The assimilation of the free electrons in the conduction band induced by fruitful doping also contributed to strong NIR absorption [25]. The NIR absorption was successfully observed with a more progressive trend as the mol % of Cu increased, as shown in Fig. 3a. The most intense absorption was executed by the 3 mol% Cu doped CdS NPs which further confirmed the successful doping of Cu^{2+} in CdS lattice and most effectively for 3 mol% dopant concentration. The resulting band gaps exhibited a significant increment exceptionally for the Cu doped CdS NCs with a prospective absolute value of 2.20 eV for 3 mol% Cu doping. The blue shift of the absorption band edge of CdS and the presence of excitonic transitions due to Cu doping indicate the quantum confinement effect. For the CdS doped with 1 % Cu, the band gap increases predominately compared to 3 % Cu doped one. Also, in the case of 5 % Cu doping, an insignificant change was observed in the band gap, leading to a higher percent of doping. This may be linked to the filling up of the conduction band edge by the excessive carriers donated by the impurity atoms and effectively leads to a blue shift in optical band-to-band transitions by blocking the low energy transitions [26,27]. Fig. 3b exhibits the green emissive photoluminescence spectra of the 1, 3 and 5 mol% Cu doped CdS NPs appeared at ~530 nm on excitation of 340 nm wavelength. The emissions related to colloidal surface passivation as prepared using BSA protein have been discussed in detail in our earlier report. Interestingly, the resulting emission exhibited a bathochromic shift of ~14 nm during successive additions of 1, 3 and 5 mol% of Cu. At the same time, consecutive increment of dopant concentration does not exhibit any shifting of the characteristics peak; instead, they are
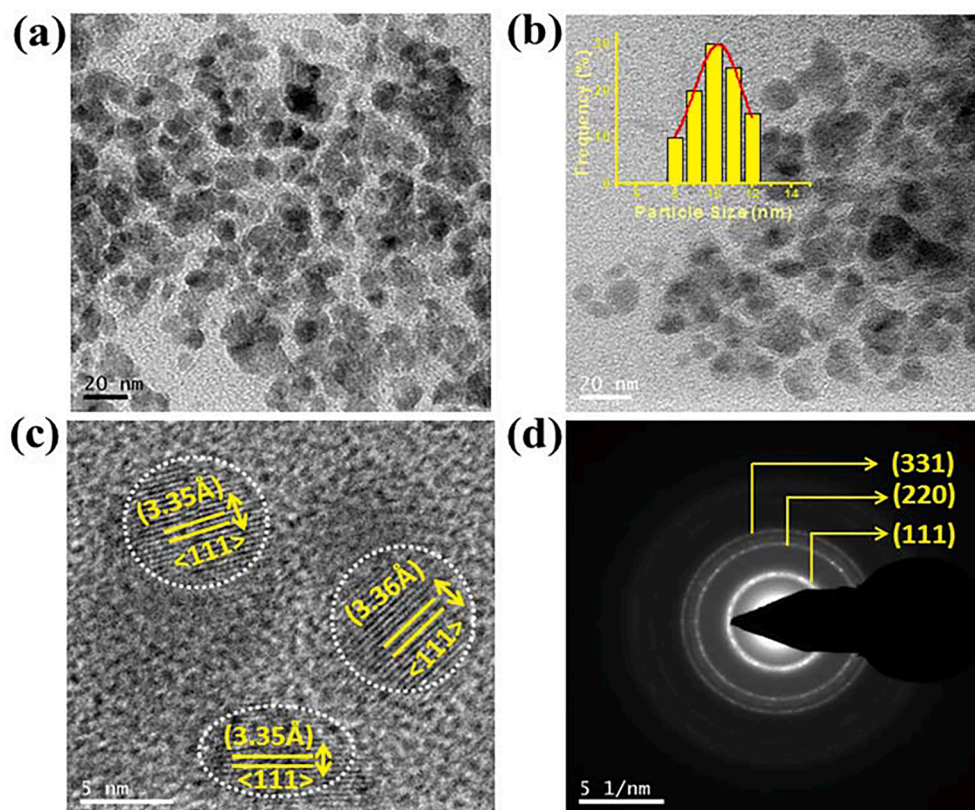
Fig. 2. (a) and (b) TEM bright-field image of 3% Cu-CdS NCs (inset of 2(b): corresponding particle size distribution histogram plot), (c) and (d) corresponding HRTEM and SAED pattern with the assigned cubic crystalline plane, respectively.
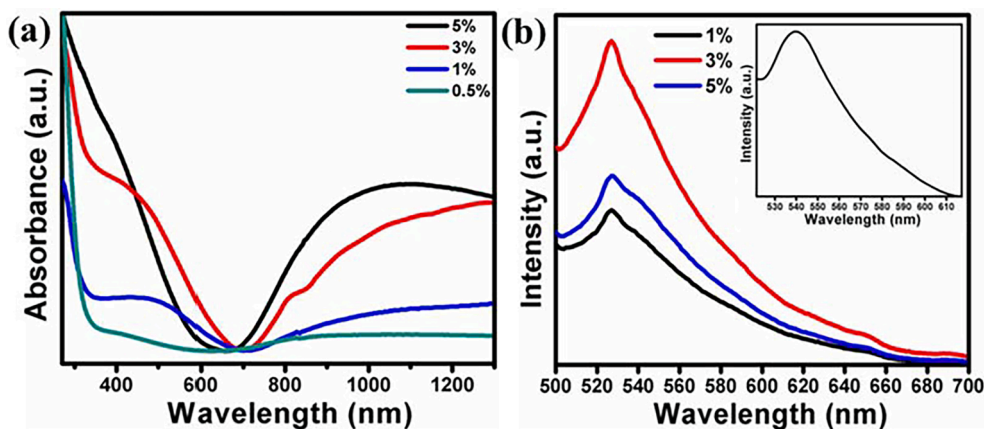
Fig. 3. (a) Absorption spectra of 0.5,1,3 and 5 mol% Cu doped CdS NCs and (b) Photoluminescence (PL) spectra of 1, 3 and 5 mol% of Cu doped CdS NCs (excitation wavelength: 340 nm) at room temperature [Inset: PL spectra of undoped CdS at the same excitation wavelength].

becoming more intense. Therefore, during Cu incorporation in the CdS lattice, an effective crystalline size enhancement was observed. It is expected that 5 % doping leads to a larger crystallite size than 1 %, indicating a successful impregnation of Cu in the CdS lattice [28]. Increment in crystallite size also affects the optical bandgap of the CdS as derived by the well-known Tauc's equation [29]. The respective crystallite size and derived band gap values have been summarized in Table 2. The optical band gap of CdS has been successively reduced by increasing the mol % of Cu doping. This also correlates reduction of crystallite size, leading to an increase in the optical band gap and vice versa due to the quantum confinement effect.[30,31] Therefore, 3 % Cu doped CdS has been the optimum doping of Cu to get an ideal bandgap with suitable crystallite size for further study.

3.4. X-ray photoelectron spectroscopy analysis

The chemical nature of the 3 % Cu doped CdS NCs was also examined by X-ray photoelectron spectroscopy (XPS) analysis, as shown in Fig. 4a–c. From the XPS spectra, it is evident that there is only the existence of Cd, S and Cu without any other impurity. Fig. 4a shows the narrow range scan of the Cd 3d core level, where two peaks corresponding to the binding energies of Cd $3d_{5/2}$ at 404.2 eV and Cd $3d_{3/2}$ at 411.6 eV, respectively, are present. The spin–orbit splitting energy of 7.4 eV is characteristic of Cd^{2+} in CdS. The position of the S $2p_{3/2}$ and $2p_{1/2}$ shows their binding energies at 160.8 and 162.7 eV, respectively (Fig. 4b), which confirms that S exists mainly in the form of S^{2-} chemical state on the sample's surface. At the same time, binding energies correspond to 930.8 and 951.2 eV assigned for strictly Cu^{2+} state, as shown in Fig. 4c. The corresponding spin–orbit splitting energy was observed at 20.4 eV, has a significant indication of the Cu^{2+} state of Cu, and highlights the presence of Cu in CdS [32]. The homogeneous distribution of Cd and S followed by the doping of Cu is very clear from the

FESEM elemental mapping analysis. This confirms the homogeneous distribution of CdSalong with doped Cu throughout the surface, as illustrated in Fig. 4d.

3.5. Studies on optical interaction of colloidal Cu doped CdS nanoparticles with the N719 dye molecule

The absorption spectrum of the N719 dye molecule exhibits broad absorption throughout the UV and visible region, as shown in Fig. 5a. The highest energy sharp absorption with maxima at ~310 nm originated from the Π → Π* intraligand transition of the corresponding dye. Besides, the metal-to-ligand charge transfer (MLCT) process leads to exhibit of visible absorptions at ~385 nm (MLCT1) and ~529 nm (MLCT2), as shown in Fig. 5a [4]. The chemical structure of N719 dye is given inset of Fig. 5a. As revealed in Fig. 5b, the synthesized 3 % Cu doped CdS NPs exhibited an emission spectrum at 530 nm. Consequently, the room temperature emission further brings the possibility of energy transfer to the N719 dye molecule as one of its absorptions appeared at 529 nm, as highlighted in the yellow colour in Fig. 5a. To understand the effect of Cu doping, we have further treated the undoped colloidal CdS with an N719 dye molecule for the comparative study. Therefore, it is predominantly active in the visible region, the major part of the solar irradiance spectrum. Hereafter, the excitation wavelength of the samples was fixed at ~330 nm to establish the resonance energy transfer dynamics in the studied systems. Fig. 5b **and** c exhibit the room temperature emission spectra of CdS nanoparticles and 3 % Cu doped CdS NCs recorded on 340 nm excitation and the absorbance spectra of the N719 dye in ethanol originating from MLCT2. The shaded zones indicate the spectral overlap of common areas in the combined normalized absorption and emission spectra in Fig. 5b and c. The significant spectral overlap of the PL spectrum of CdS and 3 mol% Cu doped CdS with the MLCT2 band of N719 dye justifies energy transfer from CdS to the N719 dye molecule. It is also noticeable here that the integral overlap area of the spectral overlap zone is higher in the case of 3 mol% Cu doped CdS than undoped CdS [33,34].

In order to demonstrate the possibility of energy transfer from CdS and Cu doped CdS to N719, the gradual quenching in the emission of the donor molecules has been studied by monitoring the emission spectra of the CdS and 3 % Cu doped CdS with increasing concentration of the acceptor sensitizers N719. The concentration of the sensitizers had been increased from 0.1 μM to 2 μM with a regular increment of 0.1 μM. It is worth mentioning the rapid quenching of the emission of the donor CdS in the event of the faster energy transfer to the acceptor N719 increasing their respective concentrations. Here is the conjugation of semiconductor CdS and N719 dye molecule's mutual collaboration to build up an energy transfer channel for DSSC as demonstrated in Fig. 6a and c.

Table 2
Crystalline size and optical band gap variation for undoped and different mol% of Cu doped CdS nanoparticles.

Sample	Crystalline size (nm) calculated from Scherrer Equation	The optical band gap (eV) derived from Tauc's plot
Only CdS	~4.2	~2.33
0.5 % Cu doped CdS	~4.8	~2.30
1 % Cu doped CdS	~5.6	~2.25
3 % Cu doped CdS	~6.0	~2.20
5 % Cu doped CdS	~6.5	~2.15
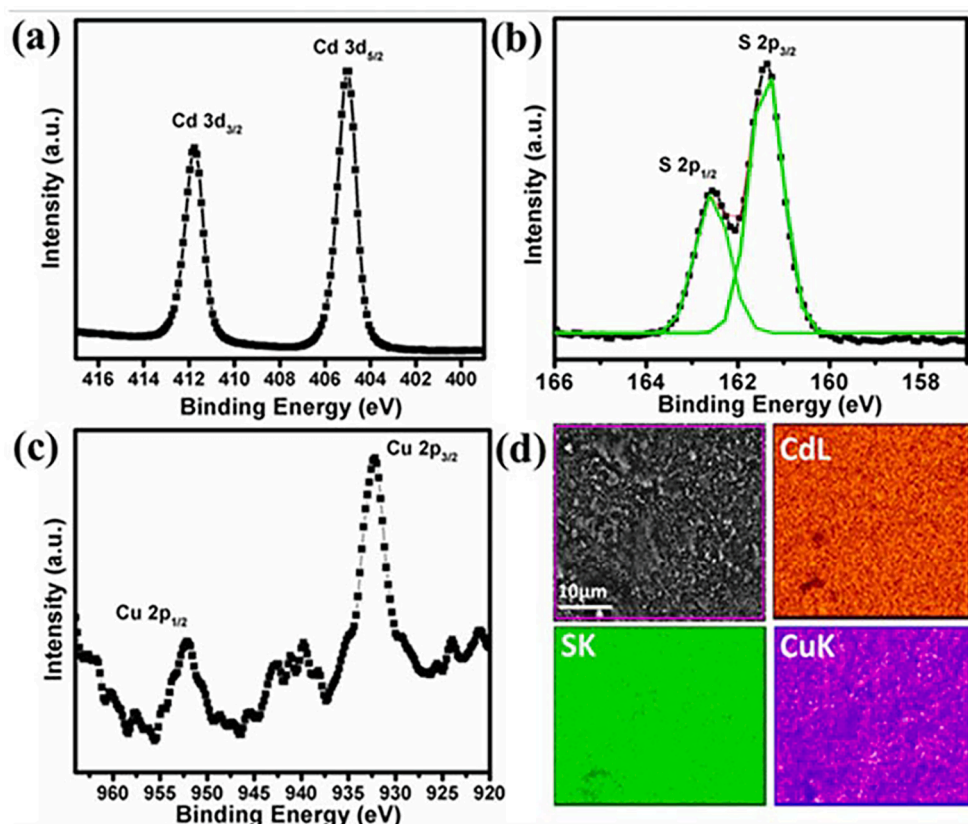
Fig. 4. Core-level XPS spectrum of 3% Cu doped CdS for (a) Cd-3d, (b) S-2p, (c) Cu-2p and (d) corresponding FESEM elemental colour mapping analysis.
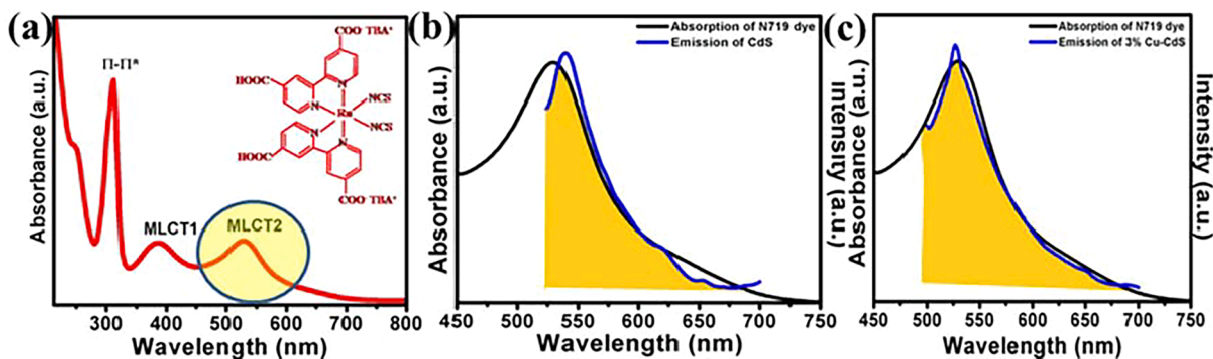
Fig. 5. (a) Absorption spectrum of N719 dye in ethanol (inset: chemical structure of N719 dye), (b) and (c) room temperature emission spectrum of CdS nanoparticles and 3% Cu doped CdS NCs with the absorption spectra of N719 (normalization of the plots has been done concerning intensity. The spectral overlap areas have been shown as the shaded zones.

Using a 1 μM concentration of N719 dye, the undoped CdS quenching saturated up to ~40 %, as shown in Fig. 6a. Whereas, in the case of 1 % Cu doped CdS, the quenching saturation rise to ~60 % in the presence of 2 μM concentrated N719 dye, as shown in Fig. 6b. Again, for the same level of quenching saturation for 3 % Cu doped CdS, a 1 μM concentration of N719 dye is fine enough to achieve the saturated condition as observed in Fig. 6c.

The ratio of the steady-state emission intensity of the donors in the absence (I_0) and presence (I) of the acceptor sensitizer has been established through Stern-Volmer (S-V) plot shown in Fig. 6(d)–(f). [S] corresponds to the concentrations of the sensitizers, and K_{SV} represents the Stern-Volmer (S-V) constant in the S-V equation shown in Eq. (i) [35].

$$I_0/I = 1 + K_{SV}[S] \qquad (i)$$

The calculated S-V constants (K_{SV}) are 0.34×10^7 M^{-1}, 0.52×10^7

M^{-1} and, 0.63×10^7 M^{-1} for undoped CdS, 1 % Cu doped and 3 % Cu doped CdS, respectively. The high K_{SV} value obtained for 3 % Cu doped CdS for the acceptor molecule N719 asserts N719 as a faster quencher towards the synthesized colloidal 3 % Cu doped CdS than 1 % Cu doped and undoped CdS.

The PL quenching mechanism provides evidence of the synthesized colloidal CdS affinity towards N719 dye [36]. It also indicates that the quenching mechanism is faster in the case of 3 % Cu doping than 1 % and certainly slower for undoped CdS in the presence of the same concentrated N719 dye molecules. The quenching processes reflect that a less concentrated acceptor is comparatively enough to saturate the PL emission quenching of the donor up to ~60 %. A digital colour-changing visual image of the sequential addition of N719 dye to 3 % Cu doped CdS solution was shown in Fig. 7a.

The average energy transfer efficiency (E) can further be calculated
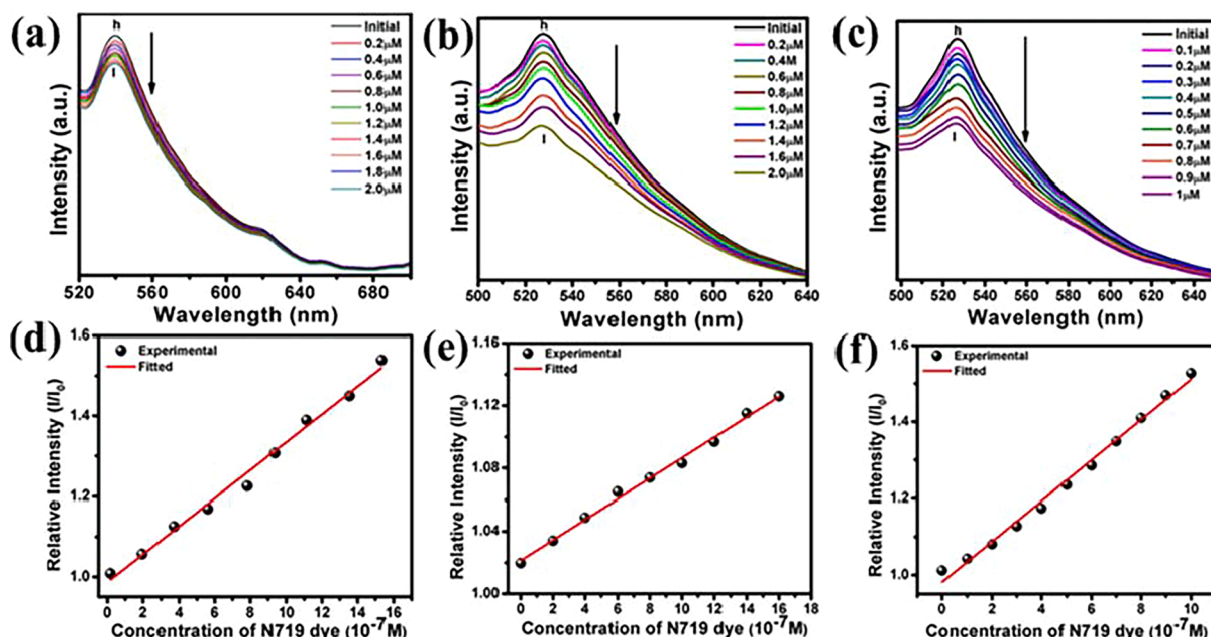
Fig. 6. (a)–(c) PL quenching spectra in the presence of a different concentrations of N719 dye solution and (d)–(f) corresponding Stern-Volmer plots for undoped, 1% Cu and 3% Cu colloidal CdS samples, respectively.

Fig. 7. Photograph of the ethanolic solution of colloidal Cu-CdS nanoparticles (donor:D) in a different concentration of N719 dye (acceptor: A) as a donor–acceptor pair.

from **Eq. (ii)** by measuring the fluorescence intensity for the donor alone and in the presence of the acceptor sensitizer.

$$E = 1 - (I_{D-A}/I_D) \tag{ii}$$

The calculated energy transfer efficiencies are found to be 61 %, 52 % and 43 % for the 3 %, 1 % Cu doped colloidal CdS and undoped colloidal CdS, respectively. The calculated energy efficiencies established the superiority in the energy transfer from the donor CdS to the acceptor N719, which becomes relatively faster with the introduction of Cu in CdS. Cu entrapment in CdS can effectively increase a maximum energy transfer rate up to ~42 % more than only CdS. This also supports the incorporation of Cu in CdS has been found quite impressive and dedicated to enhancing the optical property of CdS. The K_{SV} values and energy transfer rates for undoped and doped colloidal CdS solutions are tabulated in Table 3. Fig. 8a explains the K_{SV} and average energy efficiency relationship proportional for doped and undoped colloidal CdS. Of course, Cu doping enhances both the K_{SV} and energy efficiency for all the cases than undoped CdS, and it is saturated once the doping increases up to 5 mol %. Besides, the optimized 3 % Cu doping resulted from a predominant improvement for energy efficiency delivery towards N719 than other doped samples. Hence, in the case of 3 % Cu doping, the

Table 3
Integrated quantum yield measurement of doped and undoped CdS before and after treatment with N719 dye.

Sample	Initial QY	Decrease in QY (%)
CdS	3.1	0
With N719 (2 μM)	2.4	21.4
1 % Cu-CdS	3.4	0
With N719 (2 μM)	2.0	40.7
3 % Cu-CdS	3.6	0
With N719 (2 μM)	1.6	53.8

K_{SV} and its corresponding energy efficiency corroborate the closest relationship, as observed in Fig. 8a. Despite that, the phenomena of energy transfer from CdS towards the sensitizer N719 have been further established by measuring the fluorescence quantum yield (QY) of both doped and undoped colloidal CdS solution in ethanol in the absence and presence of the sensitizer N719. The superior energy transfer by absorbing high energy photons causes a significant role in controlling the recombination of excited electrons [37]. At the same time, allowing an indirect electron excitation source to generate more electrons towards the photoanode for a DSSC device. The QY of colloidal CdS fluorescence has been defined as the ratio of the fluorescence quanta to the number of absorbed quanta ($I_{fluorescence}/I_{absorbed}$) [38]. At the outset, the solution of 3 % Cu doped CdS in ethanol without the acceptor sensitizer exhibited a QY of ~3.6 %. Interestingly, a loss in QY of 88 % was observed, with an overall QY of ~0.4 % in the presence of N719.

In contrast, only a 48 % decrease was observed in the case of undoped CdS (fluorescence QY ~ 3.1 %), exhibiting an overall QY of ~1.8 % after being treated with acceptor N719 dye. This significant loss in QY elucidates the quenching of fluorescence due to energy transfer from the donor CdS to the acceptor sensitizers, which is due to the decrease in the fluorescence lifetime of the donor in the presence of the acceptor. The more significant loss in fluorescence quantum yield further supports the superiority in energy transfer in the donor–acceptor pair of 3 % Cu doped colloidal CdS than undoped colloidal CdS.

On the other hand, in order to explicit the dynamic nature of the fluorescence quenching of the donor by successful energy transfer towards the acceptor sensitizer by ruling out the possibility of the
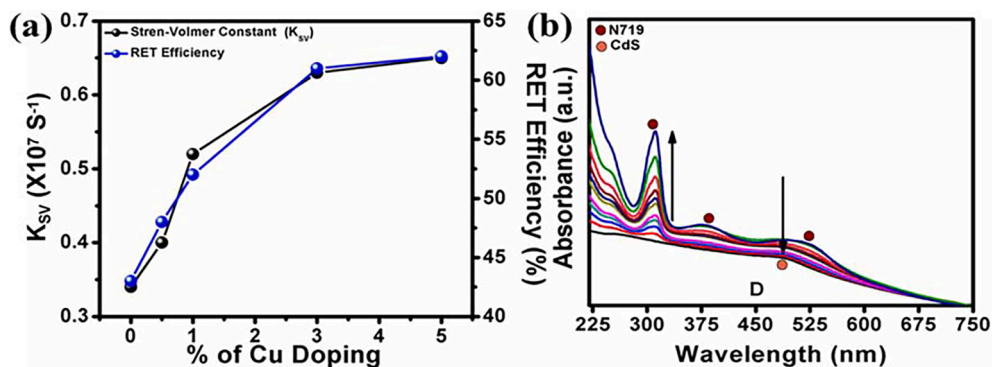
Fig. 8. (a) Stern-Volmer constant and RET efficiency plot for different molar percentages of Cu doped CdS and (b) absorption spectra of 1 mM N719 dye (fixed concentration) upon the successive addition of 3 % Cu CdS solution.

formation of any donor–acceptor complex in the ground state, the absorbance spectra of the acceptor sensitizer N719 has been measured with a valid increment of the amount of the donor 3 % Cu-CdS from a lower to higher concentration [39]. Fig. 8b exhibits absorbance spectra of 0.1 μM 3 % Cu-CdS solution, and this concentration has been successively increased up to 1 μM in a regular 0.1 μM interval to the acceptor sensitizer N719. The gradual enhancement of the light absorption of the fixed concentrated acceptor sensitizer N719 dye has been found upon successive incorporation of 3 % Cu CdS, which indicates the energy donor serves as an additional light absorber with adequate sensitization and this may further help to enhance the overall performance of a DSSC device. Though, there is still more work to complete to optimize the co-sensitization process of the CdS-N719 acceptor–donor pair with further treatment of TiO_2 photoanodes and evaluate their final performance in DSSC [40–42].

3.6. Effect of NIR extended spectral absorption

The charge separation efficiency of the photogenerated charge carriers of both the co-sensitized and only sensitized DSSC devices have been investigated by transient photocurrent responses of the same for several cycles with an on–off pulse duration of 10 s. A negligible photocurrent response in the dark is repeatedly enhanced to a considerable extent immediately once illuminated under the visible and NIR lights. In the revised manuscript, the photocurrent response was further boosted on visible + NIR illumination for all the cycles, as observed from Fig. S2a, SI. The higher photocurrent density of the co-sensitized devices compared to only N719 dye sensitized devices confirm the feasibility of more efficient separation of photogenerated electrons and holes for this particular co-sensitized DSSC device under the illumination extended to NIR.

Alternatively, the sensitised photoanodes' photocurrent- voltage characteristics were measured under visible and NIR light illumination in the applied voltage potential window of −15 V to +15 V, exhibiting Ohmic characteristics of the photoanode, as shown in Fig. S2b. SI. Besides, the co-sensitized DSSC devices exhibited a much higher photocurrent upon visible and NIR illumination than only the N719 dye. Interestingly, the photocurrent enhancement was ~45 % for 1 % Cu-CdS co-sensitized devices under visible and NIR lights. This further increased to ~60 %, ensuring a better career transfer for 3 % Cu-CdS co-sensitized devices compared to N719 dye sensitized devices. The entire process was repeated under the illumination of solely visible light, where a slower trend of photocurrent enhancement was found for all the devices. This result certifies the role of NIR light and the spectral absorption effect of co-sensitized DSSC devices on its PCE.

3.7. Photovoltaic performance and external quantum efficiency measurements of the co-sensitized devices

The energy transfer process for Cu-CdS nanoparticles with N719 dye molecules was examined through their PV performances, as shown in Table 4. It has been observed that co-sensitized devices exhibit better PV performance compared to only N719 dye and Cu-CdS devices.

The highest photoconversion efficiency (PCE) was achieved for 3 % Cu-CdS with N719 dye molecules ~8.17 %.. In contrast, the PCE was around 7.32 % for 1 % Cu-CdS nanoparticles, as shown in Fig. 9a. Co-sensitized devices resulted in ~31 % PCE improvement compared to only dye-sensitized devices. Besides, the PCE improvement for co-sensitzied devices was also drastically boosted (>100 %) in the case of only Cu-CdS nanoparticles-sensitized devices.

An excellent photocurrent density (J_{SC}) enhancement was observed during the co-sensitization may be due to the energy transfer process as observed during their optical spectral overlap. However, similar devices experienced a significant reduction of open-circuit voltage (V_{OC}) and fill factor (FF), possibly due to the agglomeration of the dye and QD molecules during the co-sensitization process leading to an increase in the series resistance of the photoanode-sensitizer interface. High dye/sensitizer coverage refers to effective intermolecular interactions without back-electron transfer. Besides, corresponding EQE values increase up to 58 % for 3 % Cu-CdS, followed by 49 % for 1 % Cu-CdS and 35 % for only N719 dye as recorded at 530 nm (Fig. 9b). Along with the PV performance, the EQE results strongly show the advantage of co-sensitization of the devices by improving the EQE significantly to reduce electron entrapment within surface trap states or loss within the electrolyte.

3.8. Proposed mechanism of Cu doped CdS-N719 and CdS-N719 co-sensitized acceptor–donor energy transform

The proposed resonance energy transfer mechanism within the sensitizer duo for doped and undoped CdS NCs as a donor and N719 dye as an acceptor with the regular electronic transitions in the conventional DSSCs has been illustrated in Fig. 10 [6,43,44]. In conventional DSSC, harvesting sunlight mainly relies upon the sensitizers according to their absorption capability, as shown in *step1* for dye and *step 2* for

Table 4
Photovoltaic performance of the champion Cu-CdS and N719 dye co-sensitized devices compared with only N719 dye-sensitized devices.

Device	$J_{SC} \pm 0.3$ (mA/cm^2)	V_{OC} (V)	FF	Efficiency ± 0.5
Only N719	11.96	0.71	0.63	6.21
Only Cu: CdS (3 %)	3.71	0.64	0.62	1.43
N719 + 1 % Cu:CdS	13.22	0.71	0.62	7.32
N719 + 3 % Cu:CdS	17.02	0.70	0.62	8.15
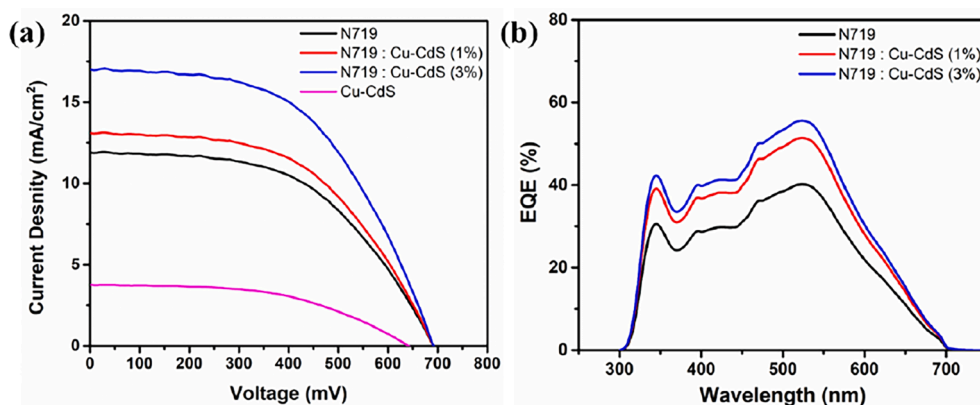
Fig. 9. (a) Current density vs voltage and (b) corresponding external quantum efficiency plot for the Cu-CdS and N719 dye co-sensitized devices compared with only N719 dye-sensitized devices.
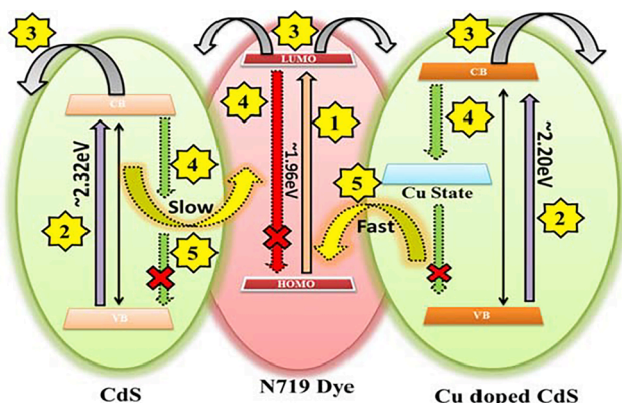
Fig. 10. Schematic representation of plausible resonance energy transfer mechanism between CdS and Cu-doped CdS nanoparticles with N719 dye molecules as a donor–acceptor pair in DSSC.

semiconductor-based sensitizers in Fig. 10. Consequently, there occurs an electronic transition from the ground state (highest occupied molecular orbital, HOMO) to the excited state (lowest unoccupied molecular orbital, LUMO) of the sensitizer dyes (Fig. 10, *step 1*). The sensitized dye further injects electrons into the conduction band of the semiconducting CdS based co-sensitizers (Fig. 10, *step 3*). The injected electron flows through the semiconducting oxide film until it reaches the attached conducting substrate contact, which is delivered to the external electrical circuit. Again, there is a possibility of recombining the excited electrons to the respective ground states if the sensitizers are shown in Fig. 10, *step 4*. During the time of excited electron release, photoluminescence of the semiconductor sensitizer can be indirectly absorbed by the dye sensitizer through RET process, as shown in Fig. 10, *step 5*. The rate of this resonance energy transfer process strictly depends on the overlapping distance between the donor's emission and the acceptor's absorption. Also, for this case, Cu incorporation causes the existence of the virtual state in the original band gap of CdS. Due to the presence of this virtual state, the emission energy released from here could be captured by the N719 dye faster than only CdS. This energy replacement varies upon placement of the virtual state for different Cu doping. This resonance energy transfer could reduce both sensitisers' recombination rate of excited electrons. At the same time, this energy is transferred as an indirect absorption of the sensitizer dye and supplies more electrons to the photoanode material for enhancing photocurrent production. Also, Cu doping enhances the light-harvesting power to the NIR region of the solar spectrum. The prepared doped and undoped colloidal CdS can absorb sunlight from UV to NIR. So without hampering the

performance of DSSC through the conventional way, this synergistic property in Step 5 of colloidal CdS makes a supplementary mode for harvesting high energy photon in the UV region without using any additional sensitizers or imposing other conditions and guide the device to perform more efficiently by successfully utilizing the additional solar spectrum. The emission generated from CdS and/or Cu doped CdS allows an indirect excitation to N719 dye, indirectly reducing the recombination rate and promoting a higher electron to the LUMO of the dye. This emission transfer as excitation energy can be termed RET (*step 5*) between the donor–acceptor pair in the case of the DSSC system. An attempt has been executed to merge the dye-semiconductor sensitizers system as acceptor–donor pairs to improve the efficiency of traditional N719 dye with CdS.

Co-sensitization causes agglomeration on the photoanode's surface, reducing the electron mobilization rate. Though the co-sensitization process seems to be an effective tool for improving conversion efficiency, some demerits are associated with the process. Perhaps the devices' traditional iodine/tri-iodide electrolyte quenches the donor's fluorescence during the co-sensitization process, limiting the device's performance. Agglomeration of dye molecules during the sensitization can be eliminated with π-spacer units in DSSCs [45]. These issues are to be solved for efficient photons extraction through new dyes and acceptor–donor pairs that extend the strategy of effective energy transfer process to facilitate the PV performance of the device. Despite possessing excellent properties and good PCE, a single organic dye is still modest compared to metal-complex dyes due to the narrow region of absorption in the visible spectrum, hence suffers the drawback of limited light-harvesting. Consequently, it limits the PCE of the DSSCs.

4. Conclusion

Colloidal Cu doped CdS has been synthesized using Bovine Serum Albumin mediated route by a sonochemical method. This has been introduced as an alternative co-sensitization through a resonance energy transfer process between CdS (donor) emission and N719 (acceptor) absorption. Cu doping causes excellent tuning of visible to NIR absorption for a single semiconductor sensitizer for maximum solar light harvesting. Remarkably 3 % Cu doping causes enhancement of optical properties of the donor–acceptor pair than other doping. A systematic photoluminescence quenching mechanism has been followed to understand the energy efficiency calculation. With this, a maximum 61 % energy transfer efficiency has been achieved with a high Stern-Volmer constant of 0.63×10^7 M^{-1} for 3 % Cu-CdS NP with N719 dye. 53 % of integrated quantum yield decrement supports emission energy transfer of 3 % Cu doped CdS to N719 dye. It is also noticeable that Cu doped enhances the energy transfer process by 40 % more than only CdS NPs. TiO_2-based photoanode exhibits 76 % PCE improvement during the co-

sensitization of 3 % Cu-CdS nanoparticles with N719 dye molecules compared to only N719 dye-sensitized devices.

Cosensitization is an effective approach to enhance the photovoltaic properties of the DSSCs through a combination of two or more dyes (having complementary absorption bands) sensitized on a semiconductor film. In contrast, fill factor of the co-sensitized devices experienced a significant reduction, whereas the corresponding photocurrent density of the devices dominates the overall performance. This will be a new way of co-sensitization and relating the popular sensitizers of DSSC-QDSSC, which may be implemented as an effective sensitizer for higher photocurrent production for a DSSC-based device.

CRediT authorship contribution statement

Anurag Roy: Writing – original draft, Investigation, Data curation. **M.J.S. Mohamed:** Methodology, Investigation, Formal analysis. **M.A. Gondal:** Writing – review & editing, Project administration, Funding acquisition. **Tapas K. Mallick:** Supervision, Resources. **Asif Ali Tahir:** Investigation, Visualization, Editing. **Senthilarasu Sundaram:** Investigation, Visualization, Editing.

Declaration of Competing Interest

The authors declare that they have no known competing financial interests or personal relationships that could have appeared to influence the work reported in this paper.

Data availability

Data will be made available on request.

Acknowledgements

Appendix A. Supplementary material

Supplementary data to this article can be found online at https://doi.org/10.1016/j.inoche.2022.110298.

References

[1] M. Kokkonen, P. Talebi, J. Zhou, S. Asgari, S.A. Soomro, F. Elsehrawy, J. Halme, S. Ahmad, A. Hagfeldt, S.G. Hashm, Advanced research trends in dye-sensitized solar cells, J. Mater. Chem. A 9 (2021) 10527–10545, https://doi.org/10.1039/D1TA00690H.

[2] K. Portillo-Cortez, A. Martínez, A. Dutt, G. Santana, N719 derivatives for application in a dye-sensitized solar cell (DSSC): a theoretical study, J. Phys. Chem. A 123 (51) (2019) 10930–10939, https://doi.org/10.1021/acs.jpca.9b09024.

[3] Y. Chi, K.-L. Wu, T.-C. Wei, Ruthenium and osmium complexes that bear functional azolate chelates for dye-sensitized solar cells, Chem. Asian J. 10 (2015) 1098–1115, https://doi.org/10.1002/asia.201403261.

[4] P.P. Das, A. Roy, S. Das, P.S. Devi, Enhanced stability of Zn₂SnO₄ with N719, N3 and eosin Y dye molecules for DSSC application, Phys. Chem. Chem. Phys. 18 (2016) 1429–1438, https://doi.org/10.1039/C5CP04716A.

[5] Y. Kusumawati, A. S. Hutama, D. V. W. R. Subagyo, Natural resources for dye-sensitized solar cells, Heliyon 7(2021) e08436. <https://doi.org/10.1016/j.heliyon.2021.e08436>.

[6] S. Ananthakumar, D. Balaji, J. Ram Kumar, S.M. Babu, Role of co-sensitization in dye-sensitized and quantum dot-sensitized solar cells, SN, Appl. Sci. 1 (2019) 186, https://doi.org/10.1007/s42452-018-0054-3.

[7] X. Lin, K. Yu, G. Lu, J. Chen, C. Yuan, Atomic layer deposition of TiO₂ interfacial layer for enhancing performance of quantum dot and dye co-sensitized solar cells,

[8] A. Roy, P.P. Das, M. Tathavadekar, S. Das, P.S. Devi, Performance of colloidal CdS sensitized solar cells with ZnO nanorods/nanoparticles, Beilst. J. Nanotechnol. 8 (2017) 210–221, https://doi.org/10.3762/bjnano.8.23.

[9] A. Kaur, P. Kaur, S. Ahuja, Förster resonance energy transfer (FRET) and applications thereof, Anal. Methods 12 (2020) 5532–5550, https://doi.org/10.1039/D0AY01961E.

[10] D.A. Jones, D.S. Bradshaw, Resonance energy transfer: from fundamental theory to recent applications, Front. Phys. 7 (2019) 100, https://doi.org/10.3389/fphy.2019.00100.

[11] J. Li, L. Zhao, S. Wang, J. Hu, B. Dong, H. Lu, L. Wan, P. Wang, Great improvement of photoelectric property from co-sensitization of TiO₂ electrodes with CdS quantum dots and dye N719 in dye-sensitized solar cells, Mater. Res. Bull. 48 (2013) 2566–2570, https://doi.org/10.1016/j.materresbull.2013.03.009.

[12] S. Luo, H. Shen, Y. Zhang, J. Li, D. Oron, H. Li, Inhibition of charge transfer and recombination processes in CdS/N719 co-sensitized solar cell with high conversion efficiency, Electrochem. Acta 191 (2016) 16–22, https://doi.org/10.1016/j.electacta.2016.01.055.

[13] S. Gao, R.Q. Fan, X.M. Wang, L.S. Qiang, L.G. Wei, P. Wang, Y.L. Yang, Y.L. Wang, Advanced CdII complexes as high efficiency co-sensitizers for enhanced dye-sensitized solar cells performance, Dalton Trans. 44 (2015) 18187–18195, https://doi.org/10.1039/C5DT02951A.

[14] H. Shen, H. Lin, Y. Liu, J. Li, D. Oron, Study of quantum dot/inorganic layer/dye molecule sandwich structure for electrochemical solar cells, J. Phys. Chem. C 116 (2012) 15185–15191, https://doi.org/10.1021/jp305050w.

[15] M.A.K.L. Dissanayake, T. Jaseetharana, G.K.R. Senadeera, B.-E. Mellander, I. Albinsson, M. Furlani, J.M.K.W. Kumari, Solid-state solar cells co-sensitized with PbS/CdS quantum dots and N719 dye and based on solid polymer electrolyte with binary cations and nanofillers, J. Photochem. Photobiol. A 405 (2021), 112915, https://doi.org/10.1016/j.jphotochem.2020.112915.

[16] Y.-J. Lin, J.-W. Chen, P.-T. Hsiao, Y.-L. Tung, C.-C. Chang, C.-M. Chen, Efficiency improvement of dye-sensitized solar cells by in situ fluorescence resonance energy transfer, J. Mater. Chem. A 5 (2017) 9081–9089, https://doi.org/10.1039/C7TA00638A.

[17] J.M. AlGhamdi, S. AlOmar, M.A. Gondal, R. Moqbel, M.A. Dastageer, Enhanced efficiency of dye co-sensitized solar cells based on pulsed-laser-synthesized cadmium-selenide quantum dots, Sol. Energy 209 (2020) 108–117, https://doi.org/10.1016/j.solener.2020.08.091.

[18] M. Shalom, J. Albero, Z. Tachan, E. Martínez-Ferrero, A. Zaban, E. Palomares, Quantum dot-dye bilayer-sensitized solar cells: breaking the limits imposed by the low absorbance of dye monolayers, J. Phys. Chem. Lett. 1 (7) (2010) 1134–1138.

[19] P. Selvaraj, A. Roy, H. Ullah, P.S. Devi, A.A. Tahir, T.K. Mallick, S. Sundaram, Soft-template synthesis of high surface area mesoporous titanium dioxide for dye-sensitized solar cells, Int. J. Energy Res. 43 (2019) 523–534, https://doi.org/10.1002/er.4288.

[20] P. Nag, P.P. Das, A. Roy, P.S. Devi, Iron antimonate quantum dots exhibiting tunable visible light emission, New J. Chem. 41 (2017) 1436–1446, https://doi.org/10.1039/C6NJ02767A.

[21] J. Santos-CruzLath, L. Marasamy, R. Manisekaran, S.A. Mayen-Hernandez, F. De Moure-Flores, R. Aruna-Devi, Divulging the role of Cu doped CdS nanocrystals as an electron acceptor in hybrid solar cells, Mat. Lett. 312 (2022), 131179, https://doi.org/10.1016/j.matlet.2022.131719.

[22] M. Rabiei, A. Palevicius, A. Monshi, S. Nasiri, A. Vilkauskas, G. Janusas, Comparing methods for calculating nano crystal size of natural hydroxyapatite using X-ray diffraction, Nanomaterials 10 (2020) 1627, https://doi.org/10.3390/nano10091627.

[23] W.T. Salam, M. Ikram, I. Shahzadi, M. Imran, M. Junaid, M. Aqeel, S. Anjum, A. Shahzadi, H. Afzal, U. Sattar, A. Asghar, A. Wahab, M. Naz, M. Nafees, S. Ali, Doping dependent structural, optical, thermal and catalysis properties of synthesized cadmium sulfide nanoparticles, Nanosci. Nanotechnol. Lett. 10 (12) (2018) 1662–1670.

[24] B. Sharma, R. Lalwani, R.A. Das, A comprehensive study of structural, optical and electrical properties of Cu doped CdS nanocrystalline thin films: for optoelectronic applications, J. Mater. Sci.: Mater. Electron. 33 (2022) 11601–11612, https://doi.org/10.1007/s10854-022-08132-w.

[25] C. Li, P. Wu, Cu-doped quantum dots: a new class of near-infrared emitting fluorophores for bioanalysis and bioimaging, Luminescence 34 (8) (2019) 782–789, https://doi.org/10.1002/bio.3679.

[26] J. Dai, Z. Suo, Z. Li, S. Gao, Effect of Cu/Al doping on electronic structure and optical properties of ZnO, Results Phys. 15 (2019), 102649, https://doi.org/10.1016/j.rinp.2019.102649.

[27] W. Li, J. Zhang, J. Wang, J. Zhang, Z. Li, Y. Yang, L. Zhang, Comparison of copper and aluminum doped cobalt ferrite nanoparticles for improving biohydrogen production, Bioresour. Technol. 343 (2022), 126078, https://doi.org/10.1016/j.biortech.2021.126078.

[28] A.A. Aboud, A. Mukherjee, N. Revaprasadu, A.N. Mohamed, The effect of Cu-doping on CdS thin films deposited by the spray pyrolysis technique, J. Mater. Res. Technol. 8 (2) (2019) 2021–2030, https://doi.org/10.1016/j.jmrt.2018.10.017.

[29] M.K.A. Mohammed, Studying the structural, morphological, optical, and electrical properties of CdS/PbS thin films for photovoltaic applications, Plasmonics 15 (2020) (2020) 1989–1996, https://doi.org/10.1007/s11468-020-01224-5.

[30] Y.V. Kuznetsova, I.D. Povov, Design and technological aspects of novel CdS quantum dots doped glass-ceramics, Ceramic Int. 48 (13) (2022) 18972–18982, https://doi.org/10.1016/j.ceramint.2022.03.180.

[31] M. Thambidurai, N. Muthukumarasamy, S. Agilan, N. Murugan, S. Vasantha, R. Balasundaraprabhu, T.S. Senthil, Strong quantum confinement effect in nanocrystalline CdS, J. Mater. Sci. 45 (2010) 3254–3258, https://doi.org/10.1007/s10853-010-4333-7.

[32] A.N. Yadav, A.K. Singh, D. Chauhan, P.R. Solanki, P. Kumar, K. Singh, Evaluation of dopant energy and Stokes shift in Cu-doped CdS quantum dots *via* spectro-electrochemical probing, New J. Chem. 44 (2020) 13529–13533, https://doi.org/10.1039/D0NJ03004J.

[33] E. Lee, C. Kim, J. Jang, High-performance Förster resonance energy transfer (FRET)-based dye-sensitized solar cells: rational design of quantum dots for wide solar-spectrum utilization, Chem. Eur. J. 19 (31) (2013) 10280–10286, https://doi.org/10.1002/chem.201300953.

[34] R. Narayanan, M. Deepa, A.V. Srivastava, Förster resonance energy transfer and carbon dots enhance light harvesting in a solid-state quantum dot solar cell, J. Mater. Chem. A 1 (2013) 3907–3918, https://doi.org/10.1039/C3TA01601C.

[35] M.H. Gehlan, The centenary of the Stern-Volmer equation of fluorescence quenching: from the single line plot to the SV quenching map, J. Photochem. Photobiol. C: Photochem. Rev. 42 (2020), 100338, https://doi.org/10.1016/j.jphotochemrev.2019.100338.

[36] M.A. Jhonsi, A. Kathiravan, R. Ranganathan, Spectroscopic studies on the interaction of colloidal capped CdS nanoparticles with bovine serum albumin, Colloids Surf. B Biointerf. 72 (2) (2009) 167–172, https://doi.org/10.1016/j.colsurfb.2009.03.030.

[37] Z. Hu, X. Liu, P.L. Hernández-Martínez, S. Zhang, P. Gu, W. Du, W. Xu, H.V. Demir, H. Liu, Q. Xiong, Interfacial charge and energy transfer in van der Waals heterojunctions, Infomat 4 3 (2022) e12290.

[38] S. Pramanik, P.S. Devi, Development of N and S heteroatom co-doped stable dual emitting carbon ink in aqueous media for sensing applications, New J. Chem. 41 (2017) 10851–10859, https://doi.org/10.1039/C7NJ02430D.

[39] A. Barth, O. Opanasyuk, T.-O. Peulen, S. Felekyan, S. Kalinin, H. Sanabria, C.A. M. Seidel, Unraveling multi-state molecular dynamics in single-molecule FRET experiments. I. Theory of FRET-lines, J. Chem. Phys. 156 (14) (2022) 141501.

[40] E. Elibol, T. Demirci, Performance analysis of hybrid quantum dots sensitized solar cells consisting of CdS/CdX (X = Se, Te, SeTe) QD and bromophenol blue dye, Opt. Mater. 122 (2021) (B) 111785, https://doi.org/10.1016/j.optmat.2021.111785.

[41] M. Antuch, S.A. Grigoriev, W.M. El Rouby, P. Millet, Implementation of a TiO$_2$/N719-dye photo-anode in a DSSC and performance analysis, Russ. J. Electrochem. 56 (2020) 929–937, https://doi.org/10.1134/S102319352010002X.

[42] G.H. Carey, A.L. Abdelhady, Z. Ning, S.M. Thon, O.M. Bakr, E.H. Sargent, Colloidal quantum dot solar cells, Chem. Rev. 115 (23) (2015) 12732–12763, https://doi.org/10.1021/acs.chemrev.5b00063.

[43] D. Shrestha, A. Jenei, P. Nagy, G. Vereb, J. Szöllősi, Understanding FRET as a research tool for cellular studies, Int. J. Mol. Sci. 16 (4) (2015) 6718–6756, https://doi.org/10.3390/ijms16046718.

[44] O. Mohiuddin, M. Obaidullah, C. Sabah, Improvement in dye sensitized solar cells from past to present, Opt. Quant. Electron. 50 (2018) 377, https://doi.org/10.1007/s11082-018-1647-1.

[45] A. Saha, B. Ganguly, A DFT study to probe homo-conjugated norbornylogous bridged spacers in dye-sensitized solar cells: an approach to suppressing agglomeration of dye molecules, RSC Adv. 10 (2020) 15307–15319, https://doi.org/10.1039/C9RA10898J.